Monthly Notices of the ROYAL ASTRONOMICAL SOCIETY

MNRAS **472,** 828–834 (2017) doi:10.1093/mnras/stx2129
Advance Access publication 2017 August 17

Erratum: Galactic synchrotron emissivity measurements between 250° < *l* < 355° from the GLEAM survey with the MWA

by H. Su,[1,2,3★] N. Hurley-Walker,[3★] C. A. Jackson,[3] N. M. McClure-Griffiths,[4] S. J. Tingay,[3,5] L. Hindson,[6,7] P. Hancock,[3] R. B. Wayth,[3] B. M. Gaensler,[8,9,10] L. Staveley-Smith,[9,11] J. Morgan,[3] M. Johnston-Hollitt,[7] E. Lenc,[8,9] M. E. Bell,[9,12] J. R. Callingham,[8,9,12] K. S. Dwarkanath,[13] B.-Q. For,[11] A. D. Kapińska,[9,11] B. McKinley,[14] A. R. Offringa,[15] P. Procopio,[14] C. Wu[11] and Q. Zheng[7]

[1]*Key Laboratory of Optical Astronomy, National Astronomical Observatories, Chinese Academy of Sciences, Beijing 100012, China*
[2]*University of Chinese Academy of Science, 19A Yuquan Road, Beijing 100049, China*
[3]*International Centre for Radio Astronomy Research, Curtin University, Bentley, WA 6102, Australia*
[4]*Research School of Astronomy and Astrophysics, Australian National University, Canberra, ACT 2611, Australia*
[5]*Istituto di Radio Astronomia, Istituto Nazionale di Astrofisica, I-40123 Bologna, Italy*
[6]*Centre for Astrophysics Research, School of Physics, Astronomy and Mathematics, University of Hertfordshire, College Lane, Hatfield AL10 9AB, UK*
[7]*School of Chemical and Physical Sciences, Victoria University of Wellington, PO Box 600, Wellington 6140, New Zealand*
[8]*Sydney Institute for Astronomy, School of Physics, The University of Sydney, NSW 2006, Australia*
[9]*ARC Centre of Excellence for All-sky Astrophysics (CAASTRO), Australia*
[10]*Dunlap Institute for Astronomy and Astrophysics, University of Toronto, 50 St. George Street, Toronto, ON M5S 3H4, Canada*
[11]*ICRAR University of Western Australia, Crawley, WA 6009, Australia*
[12]*CSIRO Astronomy and Space Science (CASS), PO Box 76, Epping, NSW 1710, Australia*
[13]*Raman Research Institute, Bangalore 560080, India*
[14]*School of Physics, The University of Melbourne, Parkville, VIC 3010, Australia*
[15]*ASTRON, The Netherlands Institute for Radio Astronomy, Postbus 2, 7990 AA, Dwingeloo, the Netherlands*

Key words: errata, addenda – cosmic rays – H II regions – Galaxy: structure – radio continuum: general.

This is an erratum to the paper 'Galactic synchrotron emissivity measurements between 250° < *l* < 355° from the GLEAM survey with the MWA', published in MNRAS, 465, 3163 (2017).

The conversion factor (5652.1) from Jy beam^{-1} to Kelvin was overestimated by a factor of 4 in the original publication because we used the semi-major and semi-minor axis lengths rather than the major and minor axis lengths while calculating this conversion factor. This leads to an overestimate of the emissivities by a factor of 1.1–2.7, thus resulting in overestimated parameters in our models.

The correct conversion factor is 1413.8. Our corrected emissivities are listed in Table 1, corrected comparisons with literature are presented in Table 2, and corrected model parameters are shown in Table 3. Figs 1–5 replaces the original Figs 4–8, respectively.

After correction, all average emissivities between the H II regions and the Galactic edge along the line of sight (ϵ_b) are in the range of 0.24 ∼ 0.70 K pc^{-1} with an average of 0.40 K pc^{-1} and a variance of 0.10 K pc^{-1}. The average emissivities between the H II region regions and the Sun (ϵ_f) have a large range of −12.72 ∼ 0.50 K pc^{-1} with a mean of −1.56 K pc^{-1} and a variance of 2.2 K pc^{-1}, although these are subject to an uncertainty in total power affecting ϵ_f. These numbers replace the corresponding numbers in our original abstract and the first paragraph of the original Section 3.1. Most of the emissivities between the H II regions and the Sun are negative now because the corrected brightness temperatures of H II regions are lower than their electron temperatures, fundamentally, because some flux of the largest scales is missed in our observations.

In the second paragraph in the original Section 2.1, 1 Jy beam^{-1} = 1413.8 K.

In the note of the original page 2, 1 K pc^{-1} is equivalent to 7.71 × 10^{-41} W m^{-3} Hz^{-1} sr^{-1} at 88 MHz in our observations.

The effect of the extragalactic emission (∼0.03 K pc^{-1}) on our measurements is smaller than our minimum error (0.05 K pc^{-1}) and smaller than our average error (0.06 K pc^{-1}). This replaces the last sentence in the third paragraph in the original Secion 3.1.

According to the brightness temperature spectrum $T(\nu) \propto \nu^{-2.3}$ (Guzmán et al. 2011) and the typical emissivity of 0.01 K pc^{-1} (Beuermann, Kanbach & Berkhuijsen 1985) at 408 MHz (Haslam et al. 1982), the typical emissivity at 88 MHz is expected to be 0.34 K pc^{-1}. The mean of our measured emissivity (ϵ_b) of 0.40 K pc^{-1} with a variance of 0.10 K pc^{-1} agrees within 1σ with this estimation. To check for any systematic differences between the samples, we compare the measurements for two H II regions that appear both in our sample and N06, in Table 2. Using the same distances and electron temperatures as listed in N06, and scaling our measurements from 88 to 74 MHz using a brightness temperature spectral index of 2.3 ($T_\nu \propto \nu^{-2.3}$, Guzmán et al. 2011), our measurements agree within 1.5σ, 0.1σ, and 5σ with those in N06 for the three matched H II regions respectively. The difference in the last pair may be due to the low brightness temperature in the surrounding region in our observations. This paragraph replaces the first and second ones in the original Section 3.2.

The results of modelling are shown in Table 3. The Uniform model shows an average emissivity of $0.38^{+0.04}_{-0.02}$ K pc^{-1} with a poor reduced chi-square ($\chi^2_{\rm red} = 6.51$). The Gaussian and Exponential models have similarly poor fits ($\chi^2_{\rm red} \sim 6.03$ and 5.77).

★ E-mail: hongquan.su@icrar.org (HS); nhw@icrar.org (NH-W)

Table 1. Corrected emissivity measurements for H II regions with absorption features. This table replaces Table 1 in the original paper.

WISE name	I_o	I_t	T_o	T_t	D_f	T_e	ϵ_f	ϵ_b	Q	Ref.
	Jy beam^{-1}	Jy beam^{-1}	$\times10^3$ K	$\times10^3$ K	kpc	$\times10^3$ K	K pc^{-1}	K pc^{-1}		
(1)	(2)	(3)	(4)	(5)	(6)	(7)	(8)	(9)	(10)	(11)
G317.988−00.754	1.86 ± 0.14	2.80 ± 0.14	2.63 ± 0.20	3.96 ± 0.20	3.6 ± 1.1	4.60 ± 0.37	−0.55 ± 0.20	0.27 ± 0.03	6	5;5
G322.036+00.625	1.30 ± 0.11	1.67 ± 0.11	1.84 ± 0.16	2.36 ± 0.16	3.5 ± 3.5	7.29 ± 0.33[a]	−1.56 ± 1.56	0.35 ± 0.06	2	1;2
G322.220+00.504	1.45 ± 0.14	1.72 ± 0.14	2.05 ± 0.20	2.43 ± 0.20	3.5 ± 3.5	7.29 ± 0.33[a]	−1.50 ± 1.50	0.34 ± 0.06	1	1;2
G326.270+00.783	1.49 ± 0.29	3.30 ± 0.29	2.11 ± 0.41	4.67 ± 0.41	3.0 ± 0.4	7.33 ± 0.33[a]	−1.74 ± 0.29	0.42 ± 0.03	5	1;2
G326.643+00.514	2.35 ± 0.29	3.30 ± 0.29	3.32 ± 0.41	4.67 ± 0.41	3.0 ± 0.4	7.32 ± 0.33[a]	−1.33 ± 0.25	0.37 ± 0.03	4	1;2
G327.300−00.548	1.32 ± 0.21	2.73 ± 0.21	1.87 ± 0.30	3.86 ± 0.30	3.2 ± 0.4	6.10 ± 0.36	−1.32 ± 0.22	0.35 ± 0.02	6	1,7;5
G327.991−00.087	5.12 ± 0.18	5.68 ± 0.18	7.24 ± 0.25	8.03 ± 0.25	3.6 ± 1.8	6.00 ± 0.36	0.34 ± 0.21	0.29 ± 0.03	5	5;5
G328.572−00.527	4.29 ± 0.19	5.98 ± 0.19	6.07 ± 0.27	8.45 ± 0.27	3.4 ± 0.4	7.19 ± 0.33[a]	−0.33 ± 0.13	0.41 ± 0.02	4	1;2
G331.365+00.521	3.32 ± 0.26	5.65 ± 0.26	4.69 ± 0.37	7.99 ± 0.37	11.8 ± 5.9	4.80 ± 0.34	−0.01 ± 0.04	0.53 ± 0.21	6	5;5
G332.145−00.452	3.44 ± 0.14	4.60 ± 0.14	4.86 ± 0.20	6.50 ± 0.20	3.7 ± 0.4	7.05 ± 0.32[a]	−0.59 ± 0.12	0.37 ± 0.02	4	1;2
G332.657−00.622	2.19 ± 0.39	3.68 ± 0.39	3.10 ± 0.55	5.20 ± 0.55	3.3 ± 0.4	7.15 ± 0.32[a]	−1.23 ± 0.24	0.39 ± 0.04	3	1;2
G332.762−00.595	2.18 ± 0.39	3.68 ± 0.39	3.08 ± 0.55	5.20 ± 0.55	3.8 ± 0.4	7.01 ± 0.32[a]	−1.03 ± 0.20	0.39 ± 0.04	3	1;2
G332.978+00.773	4.16 ± 0.16	5.75 ± 0.16	5.88 ± 0.23	8.13 ± 0.23	3.8 ± 0.5	4.00 ± 0.35	0.50 ± 0.13	0.27 ± 0.02	5	5;5
G333.011−00.441	2.09 ± 0.23	3.42 ± 0.23	2.95 ± 0.33	4.84 ± 0.33	3.6 ± 0.4	7.06 ± 0.32[a]	−1.14 ± 0.18	0.38 ± 0.02	5	1;2
G333.093+01.966	1.77 ± 0.24	2.57 ± 0.24	2.50 ± 0.34	3.63 ± 0.34	1.6 ± 0.6	7.67 ± 0.35[a]	−3.23 ± 1.25	0.34 ± 0.02	5	1;2
G333.627−00.199	2.42 ± 0.27	4.90 ± 0.27	3.42 ± 0.38	6.93 ± 0.38	3.2 ± 0.4	7.16 ± 0.32[a]	−1.17 ± 0.21	0.44 ± 0.03	4	1;2
G337.957−00.474	4.66 ± 0.19	5.46 ± 0.19	6.59 ± 0.27	7.72 ± 0.27	3.1 ± 1.6	5.60 ± 0.35	0.32 ± 0.22	0.27 ± 0.03	4	5;5
G338.706+00.645	3.87 ± 0.30	5.64 ± 0.30	5.47 ± 0.42	7.97 ± 0.42	4.3 ± 0.4	6.76 ± 0.31[a]	−0.30 ± 0.13	0.40 ± 0.03	4	1;2
G338.911+00.615	3.75 ± 0.30	5.64 ± 0.30	5.30 ± 0.42	7.97 ± 0.42	4.4 ± 0.4	6.73 ± 0.31[a]	−0.32 ± 0.12	0.40 ± 0.03	4	1;2
G338.934−00.067	4.62 ± 0.21	6.29 ± 0.21	6.53 ± 0.30	8.89 ± 0.30	3.2 ± 0.4	7.10 ± 0.32[a]	−0.18 ± 0.14	0.39 ± 0.02	4	1;2
G339.109−00.233	4.25 ± 0.29	5.70 ± 0.29	6.01 ± 0.41	8.06 ± 0.41	6.5 ± 3.3	4.20 ± 0.32	0.28 ± 0.16	0.29 ± 0.06	4	5;5
G339.134−00.377	3.25 ± 0.29	5.70 ± 0.29	4.59 ± 0.41	8.06 ± 0.41	3.0 ± 0.4	7.16 ± 0.32[a]	−0.86 ± 0.21	0.43 ± 0.03	3	1;2
G340.216+00.424	2.75 ± 0.30	4.71 ± 0.30	3.89 ± 0.42	6.66 ± 0.42	4.4 ± 2.2	4.80 ± 0.33	−0.21 ± 0.16	0.32 ± 0.04	6	5;5
G340.678−01.049	2.22 ± 0.28	3.81 ± 0.28	3.14 ± 0.40	5.39 ± 0.40	2.3 ± 2.3	7.38 ± 0.33[a]	−1.84 ± 1.86	0.38 ± 0.04	1	1;2
G340.780−01.022	1.89 ± 0.28	3.82 ± 0.28	2.80 ± 0.40	5.40 ± 0.40	2.3 ± 0.6	7.38 ± 0.33[a]	−1.99 ± 0.57	0.39 ± 0.03	2	1;2
G340.862−00.870	3.22 ± 0.23	4.26 ± 0.23	4.55 ± 0.33	6.02 ± 0.33	2.3 ± 2.3	7.38 ± 0.33[a]	−1.23 ± 1.25	0.35 ± 0.04	1	1;2
G341.090−00.017	3.22 ± 0.15	5.16 ± 0.15	4.55 ± 0.21	7.30 ± 0.21	3.2 ± 3.2	7.07 ± 0.32[a]	−0.79 ± 0.80	0.40 ± 0.05	3	1;2
G342.277+00.311	2.97 ± 0.33	5.25 ± 0.33	4.20 ± 0.47	7.42 ± 0.47	9.6 ± 4.8	3.90 ± 0.32	0.03 ± 0.06	0.39 ± 0.11	4	5;5
G343.480−00.043	2.46 ± 0.21	4.03 ± 0.21	3.48 ± 0.30	5.70 ± 0.30	13.4 ± 7.4	8.10 ± 0.35	−0.34 ± 0.19	0.71 ± 0.36	6	5;5
G343.914−00.646	3.71 ± 0.16	4.38 ± 0.16	5.25 ± 0.23	6.19 ± 0.23	2.8 ± 1.4	7.20 ± 0.35	−0.70 ± 0.38	0.32 ± 0.03	5	5;5
G345.094−00.779	1.72 ± 0.29	4.26 ± 0.33	2.43 ± 0.41	6.02 ± 0.47	2.1 ± 2.1	7.43 ± 0.33[a]	−2.38 ± 2.39	0.42 ± 0.04	4	1;2
G345.202+01.027	1.18 ± 0.61	4.10 ± 0.61	1.67 ± 0.86	5.80 ± 0.86	1.1 ± 0.6	4.80 ± 0.12	−2.85 ± 1.74	0.33 ± 0.05	4	4;5
G345.235+01.408	1.12 ± 0.34	2.59 ± 0.34	1.72 ± 0.48	3.66 ± 0.48	8.0 ± 4.0	6.00 ± 0.35	−0.64 ± 0.33	0.44 ± 0.09	5	2;2
G345.410−00.953	2.00 ± 0.40	3.60 ± 0.40	2.83 ± 0.57	5.09 ± 0.57	2.6 ± 0.6	6.96 ± 0.05	−1.59 ± 0.43	0.36 ± 0.03	6	1;2
G348.261+00.485	3.40 ± 0.32	6.05 ± 0.32	4.81 ± 0.45	8.55 ± 0.45	1.8 ± 1.8	7.53 ± 0.34[a]	−1.51 ± 1.55	0.43 ± 0.04	4	1;2
G348.691−00.826	2.15 ± 0.33	3.03 ± 0.33	3.04 ± 0.47	4.28 ± 0.47	3.4 ± 0.3	4.80 ± 1.00	−0.52 ± 0.33	0.24 ± 0.05	6	1;6
G348.710−01.044	1.27 ± 0.28	2.67 ± 0.28	1.80 ± 0.40	3.77 ± 0.40	3.4 ± 0.3	6.20 ± 1.00	−1.57 ± 0.18	0.37 ± 0.02	6	1;8
G350.991−00.532	3.16 ± 0.31	4.31 ± 0.31	4.47 ± 0.44	6.09 ± 0.44	13.7 ± 6.9	6.10 ± 0.35	−0.12 ± 0.07	0.53 ± 0.25	5	5;5
G350.995+00.654	2.08 ± 0.67	6.86 ± 0.67	2.94 ± 0.95	9.70 ± 0.95	0.6 ± 0.3	10.57 ± 0.34	−12.72 ± 6.58	0.62 ± 0.05	5	8;8
G351.130+00.449	2.85 ± 0.82	8.24 ± 0.82	4.03 ± 1.16	11.65 ± 1.16	1.4 ± 0.7	6.65 ± 0.07	−1.87 ± 1.25	0.53 ± 0.06	5	8;8
G351.311+00.663	2.12 ± 0.35	6.96 ± 0.35	3.00 ± 0.49	9.84 ± 0.49	1.3 ± 0.1	7.71 ± 0.35[a]	−3.63 ± 0.54	0.54 ± 0.03	3	9;2
G351.383+00.737	1.77 ± 0.34	7.02 ± 0.34	2.50 ± 0.48	9.93 ± 0.48	1.3 ± 0.1	9.70 ± 0.09	−5.54 ± 0.57	0.63 ± 0.03	5	9;2
G351.516−00.540	3.28 ± 0.30	6.04 ± 0.38	4.64 ± 0.42	8.54 ± 0.54	3.3 ± 3.3	5.70 ± 1.00	−0.32 ± 0.46	0.38 ± 0.07	3	6;3
G351.688−01.169	1.71 ± 0.25	3.87 ± 0.25	2.42 ± 0.35	5.47 ± 0.35	14.2 ± 1.0	6.49 ± 0.21	−0.29 ± 0.04	0.67 ± 0.06	6	2;2
G353.038+00.581	1.52 ± 0.56	5.33 ± 0.56	2.15 ± 0.79	7.54 ± 0.79	1.1 ± 1.1	7.78 ± 0.35[a]	−5.12 ± 5.18	0.48 ± 0.05	3	1;2
G353.076+00.287	2.06 ± 0.75	6.81 ± 0.75	2.91 ± 1.06	9.63 ± 1.06	0.7 ± 1.5	5.39 ± 0.10	−3.54 ± 7.74	0.44 ± 0.06	5	2;2
G353.092+00.857	1.29 ± 0.56	5.33 ± 0.56	1.82 ± 0.79	7.54 ± 0.79	1.0 ± 2.0	7.10 ± 0.40	−5.28 ± 10.59	0.47 ± 0.06	5	2;2

Notes: Col. (1): The name of H II regions from the WISE H II region catalogue. Cols. (2) and (3): The MWA surface brightness measurements of the absorbing H II region and the neighbouring region, respectively. Cols. (4) and (5): The brightness temperatures of the absorbing H II region and the neighbouring region, respectively. Col. (6): The distance from H II regions to the Sun found in the literature. Col. (7): The electron temperature of H II regions from the literature. Col. (8): The average emissivity from H II regions to the Sun. Note that the negative emissivities are caused by the missing flux in our observations. Col. (9): The average emissivity from H II regions to the Galactic edge. Col. (10): The indicative quality of emissivity measurements: a higher value means higher quality. Col. (11): The references for the distances and electron temperatures. The first and second number indicate the reference for the distance in Col. (6) and the electron temperature in Col. (7) respectively. The reference list: 1. Anderson et al. (2014); 2. Balser et al. (2015); 3. Caswell & Haynes (1987); 4. García et al. (2014); 5. Hou & Han (2014); 6. Nord et al. (2006); 7. Paladini, Davies & De Zotti (2004); 8. Quireza et al. (2006); 9. Reid et al. (2014).
[a]The electron temperature of this H II region is derived from the statistical relation $T_e = (4928 \pm 277) + (385 \pm 29)\ R_{\rm gal}$ from Balser et al. (2015).

The Two-circle model has the best performance compared with the other three models ($\chi^2_{\rm red} = 3.74$). It shows a high emissivity ($2.0^{+1.8}_{-1.7}$ K pc^{-1}) region near the Galactic Centre within a radius of $1.7^{+0.1}_{-0.4}$ kpc, a low emissivity ($0.30^{+0.13}_{-0.17}$ K pc^{-1}) region outside of a radius of $7.5^{+5.5}_{-2.9}$ kpc, a medium emissivity ($0.59^{+0.32}_{-0.49}$ K pc^{-1}) region between the two. This replaces the second to the fifth sentences in the ninth paragraph in the original Section 4. The 10th sentence in that paragraph is redundant and should be deleted.

The number in the last sentence in the last fourth paragraph in the original Section 4 should be $2.0^{+1.8}_{-1.7}$ K pc^{-1}.

ACKNOWLEDGEMENTS

We thank Irene Polderman for identifying the mistake that caused this erratum.

Table 2. Comparison of three emissivities measured in N06 and this work. This table replaces the original Table 2.

H II region (this work)	G351.516−00.540	G348.710−01.044	G348.691−00.826
H II region (N06)	G351.5−0.5	G348.7−1.0	G348.6−0.6
Distance (kpc, used in N06)	3.3	2.0	2.7
T_e ($\times 10^3$ K, used in N06)	5.7 ± 1.0	6.2 ± 1.0	4.8 ± 1.0
Angular diameter (arcmin, used in N06)	3.46	4.47	13.27
ϵ_b(K pc^{-1}, at 74 MHz, N06)	0.36 ± 0.06	0.36 ± 0.05	0.51 ± 0.05
ϵ_b(K pc^{-1}, scaled at 74 MHz, this work)[a]	0.45 ± 0.06	0.35 ± 0.05	0.26 ± 0.05

Note. [a]To compare our measurements with those in N06, we re-calculate our emissivities for these three H II regions using the distances and electron temperatures from N06 and scale our measurements from 88 MHz to 74 MHz using a brightness temperature spectral index of 2.3.

Table 3. Revised model parameters from corrected emissivities. This table replaces the orignal Table 3.

Model	Free parameters	$\chi^2_{\rm red}$	Degrees of freedom
Uniform	$\epsilon = 0.38^{+0.04}_{-0.02}$	6.51	46
Gaussian	$\alpha_1 = 0.71^{+0.29}_{-0.22}$, $\beta_1 = 8.2^{+5.8}_{-2.7}$	6.03	45
Exponential	$\alpha_2 = 0.94^{+0.46}_{-0.43}$, $\beta_2 = 0.11^{+0.06}_{-0.07}$	5.77	45
Two-circle	$R_1 = 1.7^{+0.1}_{-0.4}$, $R_2 = 7.5^{+5.5}_{-2.9}$	3.74	42
	$\epsilon_1 = 2.0^{+1.8}_{-1.7}$, $\epsilon_2 = 0.59^{+0.32}_{-0.49}$, $\epsilon_3 = 0.30^{+0.13}_{-0.17}$		

Note: The unit of ϵ, ϵ_1, ϵ_2, ϵ_3, α_1, and α_2 are K pc^{-1}. The unit of R_1, R_2, and β_1 are kiloparsecs. The unit of β_2 is kpc^{-1}. All the quoted errors are at 2σ level. The Gaussian model tends to the Uniform model when β_1 tends to infinity.

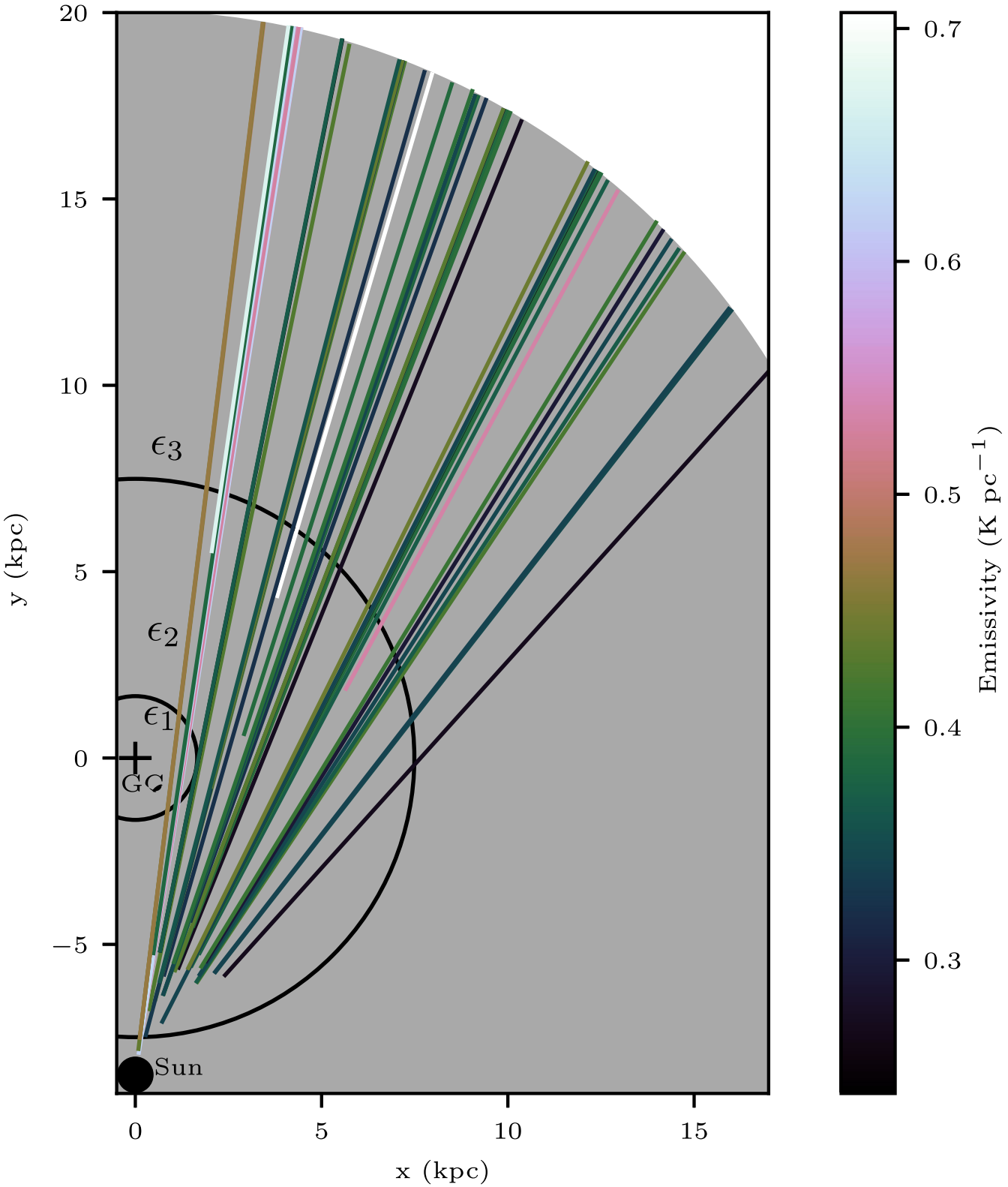

Figure 1. Distribution of emissivities (ϵ_b) on lines of sight and the Two-circle model. Each colour represents a path over which the emissivities are averaged. The colours of the lines indicate the value of emissivities along different paths. The Galactic non-thermal emission is assumed to lie in a disk with a Galactocentric radius of 20 kpc shown by the grey circle segment. The two circles near the Galactic Centre divide the Galactic plane into three regions with emissivities of ϵ_1, ϵ_2, and ϵ_3 respectively. The Galactocentric radius of the Sun is 8.5 kpc. The Sun and Galactic Centre (GC) are marked as a black dot and plus respectively. This figure replaces Fig. 4 in the original paper.

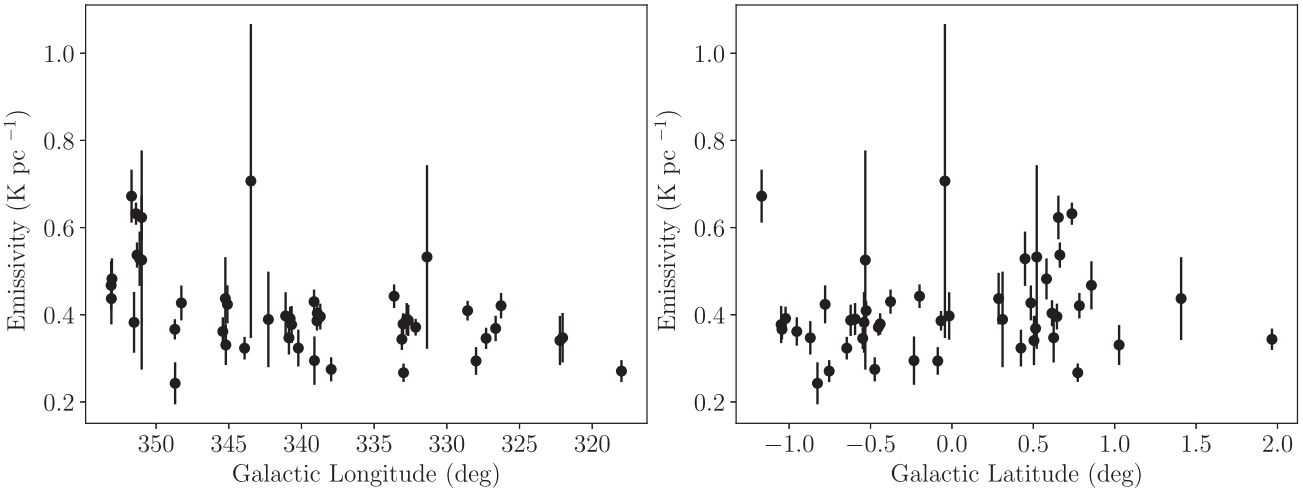

Figure 2. Distributions of emissivities (ϵ_b) with respect to Galactic longitude (left) and latitude (right). Some measurements have large errors due to the uncertainty of the distances of H II regions. This figure replaces Fig. 5 in the original paper.

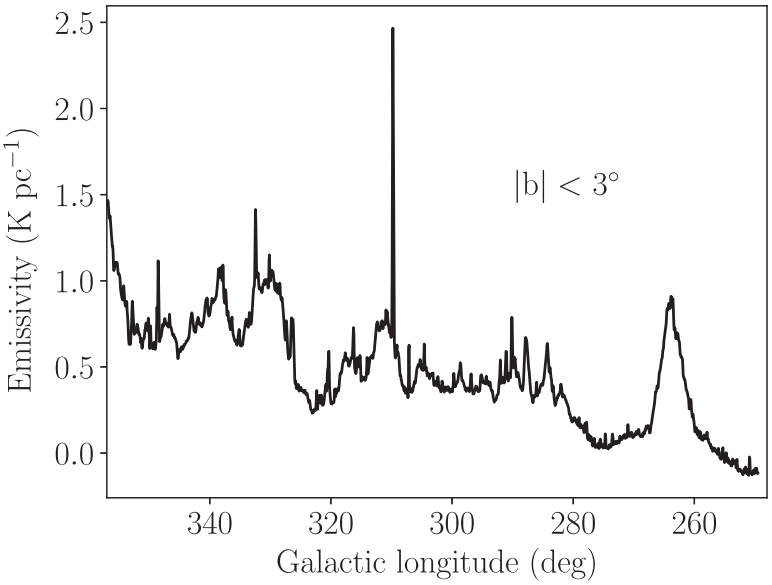

Figure 3. Distributions of emissivity from the Sun to the Galactic edge over the line of sight with respect to the Galactic longitude in the range $250^\circ < l < 355^\circ$, $|b| < 3^\circ$: this includes the contributions from point sources and supernova remnants. The bin size in Galactic longitude is $3'.75$. There is a trend of increasing emissivity with longitude. The high emissivity near the Galactic longitude 264° is contributed by the Vela supernova remnant. Note that we do not recover the total power of the Galaxy due to the interferometric nature of the measurements. This figure replaces Fig. 6 in the original paper.

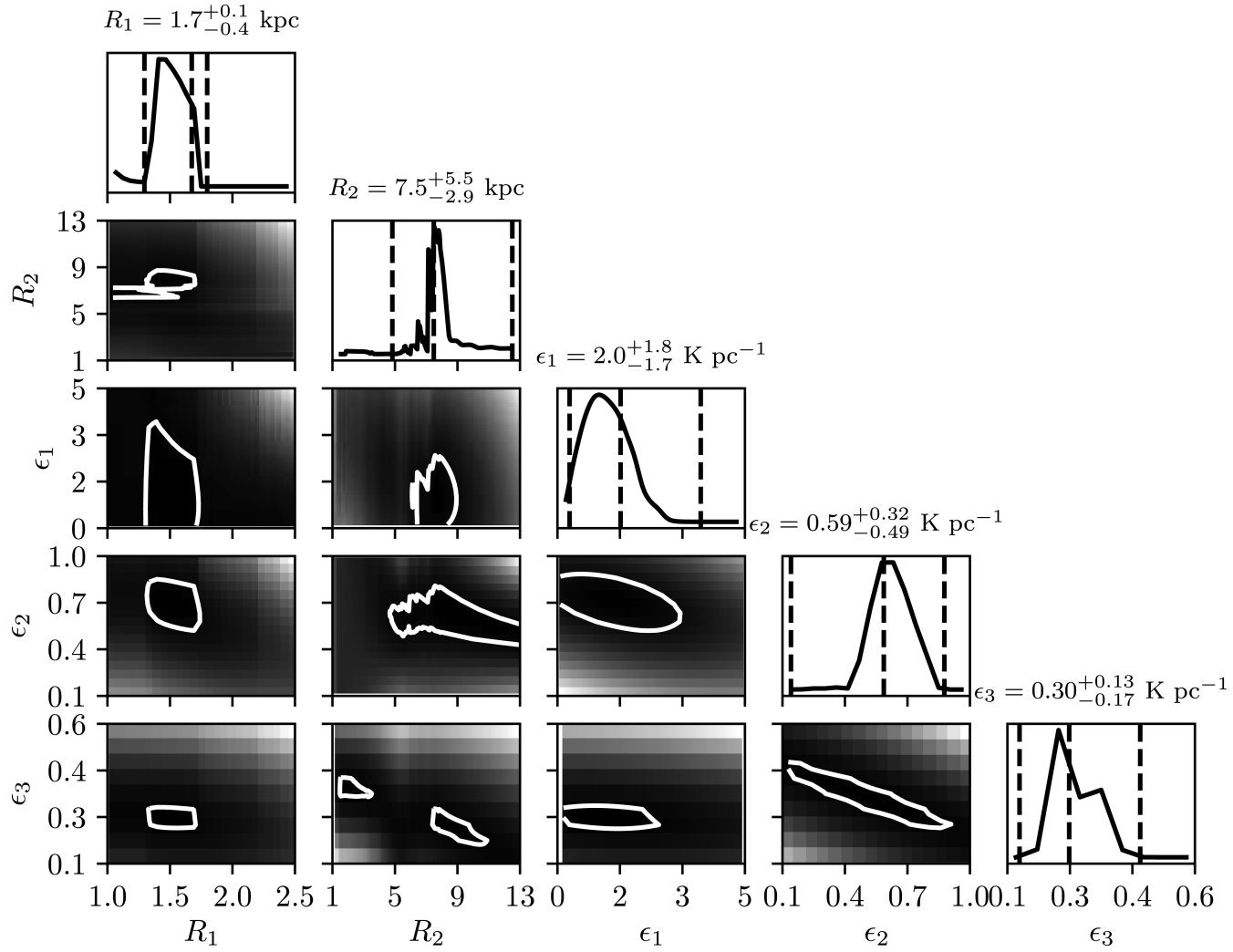

Figure 4. Triangle plot showing the correlations between the two-circle model parameters: the grey-scale traces the distributions of chi-square with darker regions indicating lower values. The 2σ boundaries of chi-square are shown by white contours. The solid black lines show the relative likelihood distributions with dashed lines showing the best values and 2σ limits of the parameters. This figure replaces Fig. 7 in the original paper.

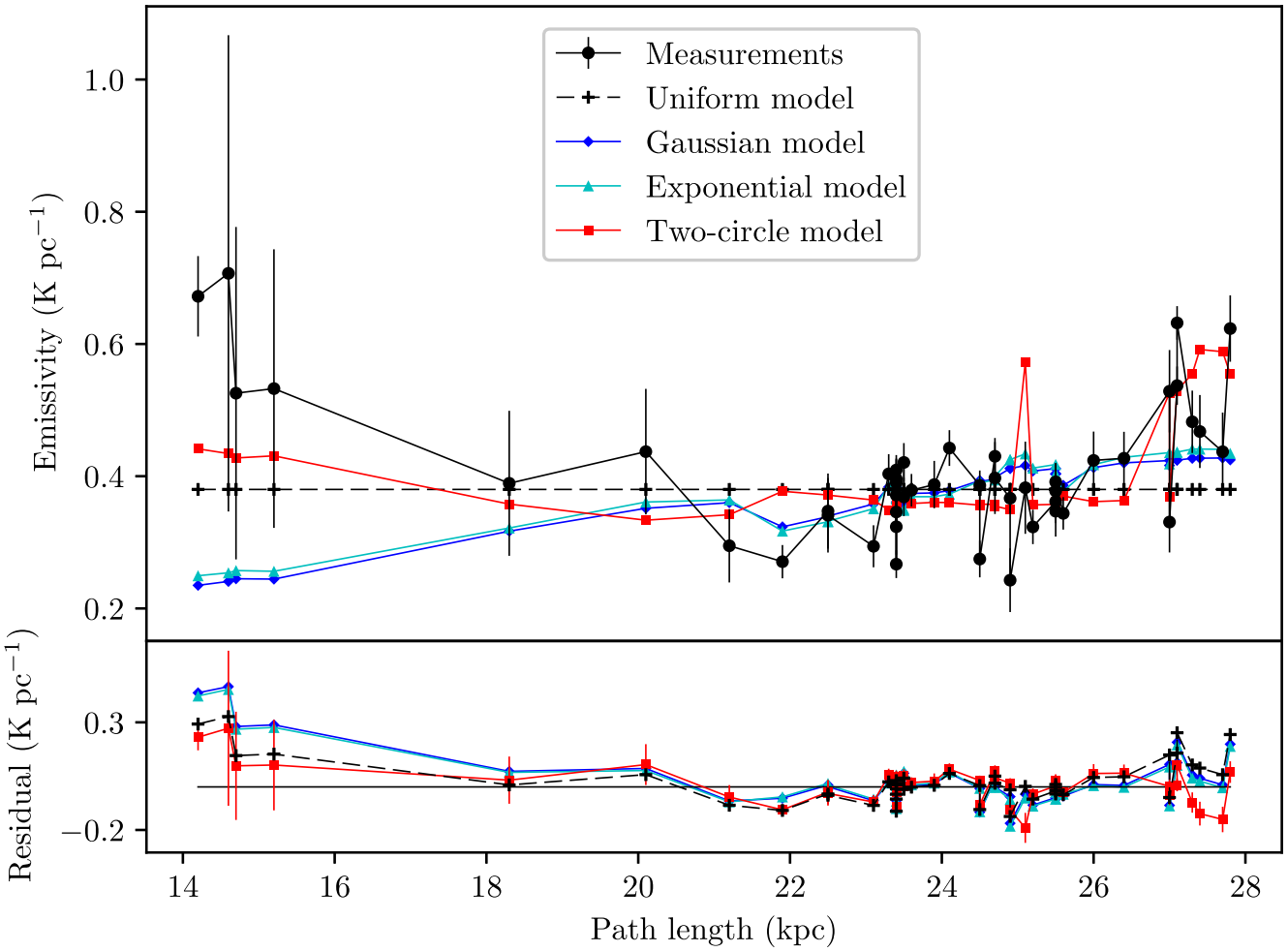

Figure 5. Distributions of emissivities (ϵ_b) from our measurements and models with the path length from H II regions to the Galactic edge along the line of sight. This figure replaces Fig. 8 in the original paper.

REFERENCES

Anderson L. D., Bania T. M., Balser D. S., Cunningham V., Wenger T. V., Johnstone B. M., Armentrout W. P., 2014, ApJS, 212, 1

Balser D. S., Wenger T. V., Anderson L. D., Bania T. M., 2015, ApJ, 806, 199

Beuermann K., Kanbach G., Berkhuijsen E. M., 1985, A&A, 153, 17

Caswell J. L., Haynes R. F., 1987, A&A, 171, 261

García P., Bronfman L., Nyman L.-Å., Dame T. M., Luna A., 2014, ApJS, 212, 2

Guzmán A. E., May J., Alvarez H., Maeda K., 2011, A&A, 525, A138

Haslam C. G. T., Salter C. J., Stoffel H., Wilson W. E., 1982, A&AS, 47, 1

Hou L. G., Han J. L., 2014, A&A, 569, A125

Nord M. E., Henning P. A., Rand R. J., Lazio T. J. W., Kassim N. E., 2006, AJ, 132, 242

Paladini R., Davies R. D., De Zotti G., 2004, MNRAS, 347, 237

Quireza C., Rood R. T., Bania T. M., Balser D. S., Maciel W. J., 2006, ApJ, 653, 1226

Reid M. J. et al., 2014, ApJ, 783, 130

This paper has been typeset from a TEX/LATEX file prepared by the author.